EDGE ARTICLE

Check for updates

A highly unsaturated six-vertex amido-substituted silicon cluster†

Jan Keuter,[a] Christian Schwermann, [ID][b] Alexander Hepp,[a] Klaus Bergander,[c] Jörn Droste, [ID][d] Michael Ryan Hansen, [ID][d] Nikos L. Doltsinis, [ID] *[b] Christian Mück-Lichtenfeld [ID] *[c] and Felicitas Lips [ID] *[a]

Thermal treatment of the bicyclo[1.1.0]tetrasilatetraamide [$Si_4\{N(SiMe_3)Dipp\}_4$] **1** resulted in the formation of a highly unsaturated six-vertex silicon cluster [$Si_6\{N(SiMe_3)Dipp\}_4$] **2** with only four amine-substituents and two ligand-free silicon atoms. In solution, a major and a minor conformer of this cluster are in equilibrium according to multinuclear NMR spectroscopy, lineshape analysis, DFT calculations and molecular dynamics simulations. The bonding situation in the highly unsaturated cluster features lone pair type character at the ligand-free silicon atoms and partial single and double bond character in the upper butterfly-shaped ring of **2**. This allows to consider **2** as the silicon analogue of a butalene isomer.

Introduction

Silicon analogues to benzene were successfully isolated with sterically demanding substituents. Isomers with a prismatic silicon scaffold **A**,[1] a benzvalene-type isomer **B**,[2] a tricyclic species **C**[3] and a propellane-type compound **D**[4] turned out from these investigations.

Computational investigation into Si_6H_6 isomers[5] revealed the spherical propellane-type compound **D**, recently termed benzpolarene,[6] to be the global minimum structure and to be much lower in energy than benzene-, benzvalene-, prismatic- or Dewar-benzene-type isomers.

In the isolated silicon analogues of benzene as well as in the computationally investigated Si_6H_6 isomers, silicon atoms with no substituent occur that are only connected to other silicon atoms. These so-called unsubstituted or "naked" silicon atoms display inverted tetrahedral[7] or hemispheroidal configurations.[8] Therefore, the topology of these clusters resembles surface structures of bulk silicon or silicon nanoparticles.[9] This type of clusters is named siliconoids[1b,8] in analogy to metalloid clusters[10] and can further be considered as model compounds
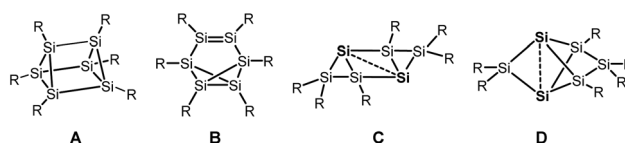
for intermediates of the chemical vapour deposition process of molecular silane precursors.[11]

Besides the six-vertex clusters depicted in Scheme 1, five-vertex silicon clusters with one **E**[12] or two ligand-free atoms **F**,[13] seven-vertex **G**[14] and **H**[15] and eight-vertex siliconoid clusters **I**[16] and **J**[17] are reported in the literature (Scheme 2).

Recent progress in this field includes a systematic stepwise synthesis from a six- to an eight-vertex siliconoid cluster,[14] and thermolysis of a siliconoid cluster into novel seven and eight-vertex silicon clusters.[15] Furthermore, functionalization of the benzpolarene-type cluster **D** at different positions[6,18] and the introduction of boron- and phosphorous-based groups, which corresponds to n- and p-type doping of elemental silicon, was achieved.[19]

Unsaturated isomers of benzene with the formula C_6H_4 were considered computationally and feature structural motifs shown in Scheme 3.[20]

Considering the lower tendency of silicon to form π-bonds and the above mentioned observation for the preference of silicon clusters for spherical scaffolds with a high number of σ-bonds, we expect a silicon analogue to C_6H_4 to adopt a Si_6 structural motif that differs from the carbon-based isomers shown in Scheme 3. Previous computational investigations using Car–Parrinello molecular dynamics simulations[21] and

[a]Westfälische Wilhelms-Universität Münster, Institut für Anorganische und Analytische Chemie, Corrensstraße 28-30, 48149 Münster, Germany

[b]Westfälische Wilhelms-Universität Münster, Institut für Festkörpertheorie, Center for Multiscale Theory and Computation, Wilhelm-Klemm-Straße 10, 48149 Münster, Germany

[c]Westfälische Wilhelms-Universität Münster, Organisch-Chemisches Institut, Center for Multiscale Theory and Computation, Corrensstraße 40, 48149 Münster, Germany
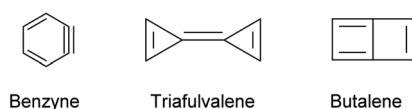
[d]Westfälische Wilhelms-Universität Münster, Institut für Physikalische Chemie, Corrensstraße 30, 48149 Münster, Germany

Scheme 1 Six-vertex silicon clusters.
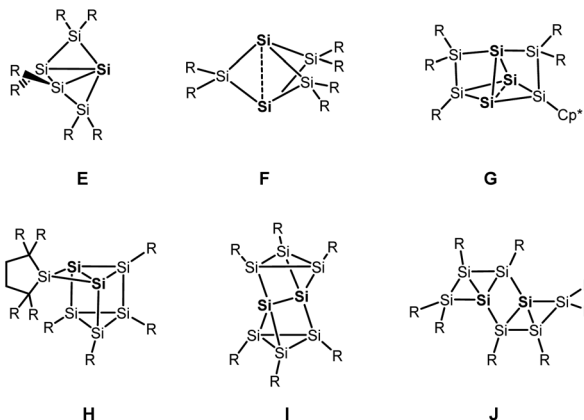
Scheme 2 Other silicon clusters with hemispheroidal silicon atoms (highlighted in bold).

Scheme 3 Possible C_6H_4 isomers.

Benzyne   Triafulvalene   Butalene

DFT calculations[22] suggested a structure with spherical scaffold for Si_6H_4. However, no such compound has been isolated yet.

Results and discussion

The silicon clusters mentioned in the introduction have the common feature that they are surrounded either by aryl, alkyl or silyl substituents. However, reports on unsaturated main group clusters with higher nuclearity stabilized by amine substituents are rare.[23] One such compound is the metalloid cluster $Sn_{15}\{N(SiMe_3)Dipp\}_6$ featuring eight ligand-free tin atoms, that was synthesized in a reductive dehalogenation of the dimeric $[\{N(SiMe_3)Dipp\}SnCl]_2$ using KC_8 as the reducing agent.[24] Recently, we reported on the bicyclo[1.1.0]tetrasilate-traamide $Si_4\{N(SiMe_3)Dipp\}_4$ **1** displaying two three-coordinate silicon atoms with different degree of pyramidalization.[25] By thermal treatment of **1** at *ca.* 400 °C under argon, removal of all volatile components *in vacuo* at 400 °C, and subsequent extraction of the yellow residue in hexane at room temperature, we were able to synthesize the first amido-substituted highly unsaturated silicon cluster $Si_6\{N(SiMe_3)Dipp\}_4$ **2** in form of yellow crystals in *ca.* 23% yield (see Scheme 4).
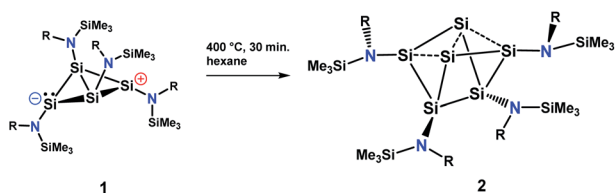
Scheme 4 Synthesis of the amido-substituted silicon cluster **2**.

Compound **2** was also obtained in much lower yield in a co-reduction of $\{N(SiMe_3)Dipp\}SiBr_3$ and $SiBr_4$ in a 2 : 1 ratio with potassium graphite (KC_8). In this case, however, **2** co-crystallized with **1**. The formation mechanism of **2** is unclear due to the difficulty to assign side products at 400 °C. Two possible formation pathways that proceed under release of bis(amido)-substituted silylene are suggested in the ESI (page S48).† The formation of siliconoid clusters **H** and **J** was also found to proceed with silylene elimination.[15] Single crystal X-ray diffraction revealed that in **2**, a Si_6 cluster core with two unsubstituted silicon atoms is surrounded by four $\{N(SiMe_3)Dipp\}$-substituents. All silicon atoms in **2** are fourfold-coordinated. The Si_6 cluster core in **2** resembles to the six-vertex propellane- or benzpolarene-type cluster **D**, but can also be considered as a heavily distorted octahedron missing two edges or as a twisted trigonal prism (see Fig. 1, bottom). The distance between the two unsubstituted silicon atoms (Si2, Si4) amounts to 2.636(6) Å which is very similar to the distance between atoms of this type in the propellane-type clusters **D** (2.708 Å) and **F** (2.636 Å). These two unsubstituted silicon atoms are part of a butterfly-shaped moiety of the cluster constituted by Si1–Si4. Within this unit the two bond lengths Si1–Si2 and Si3–Si4 (2.281(5) Å and 2.292(6)) are very short for Si–Si single bonds and approach the value reported for Si=Si double bonds (2.138–2.289 Å).[26] In contrast, the bond lengths Si2–Si3 and Si1–Si4 (2.502(6) and 2.532(6) Å) are longer than typical single bonds (2.34 Å). The butterfly-shaped moiety is capped by a dumbbell consisting of Si5 and Si6 (2.357(1) Å). The bond lengths Si2–Si6 and Si4–Si5 (2.403(6) and 2.389(6) Å) connecting the butterfly-
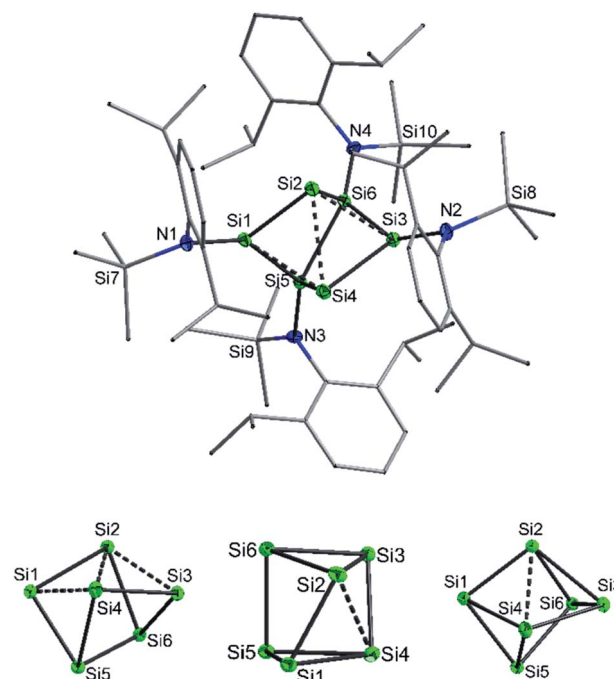
Fig. 1 (Top) Molecular structure of **2** (top view, Dipp and $SiMe_3$ groups represented as wires for clarity). (Bottom) Cluster core of **2** in three different views illustrating the close similarity to a twisted prismane and a distorted octahedron missing two edges.

type ring and the Si5–Si6-dumbbell are somewhat elongated compared to the standard Si–Si single bond length. All other bond lengths are in the range of usual single bonds. The Si–N bond lengths (1.730(1)–1.740(1) Å) are only somewhat shorter than single bonds (*ca.* 1.76 Å).[27]

We were interested to compare the configuration of the unsubstituted silicon atoms in **2** with those in the propellane-type clusters **F** and **D** in the solid state (see Fig. 2). In the propellane-type clusters the bond angles around the ligand-free silicon atoms are all *ca.* 90° in **F** and 97°, 97°, and 76° in **D**.

Thus, the configuration at the unsubstituted silicon atoms is inverted tetrahedral or hemispheroidal in **F** and **D**. This is a common feature of "naked" Si atoms as it was analyzed by Ishida and Iwamoto[7] and by Scheschkewitz.[8]

Measuring these angles in **2** results in significantly different angles of 57°, 83°, and 103°, which allows to describe the configuration of the unsubstituted Si atoms (Si2, Si4) in **2** as hemispheroidal with a hemispheroidality parameter $\varphi = 1.45$ Å. This represent the highest hemispheroidality parameter so far observed for silicon clusters.[8] More specifically, the environment at Si2/Si4 can be considered as the apical position of a distorted square-based pyramid. A persila-pyramidane was not reported yet, but was investigated computationally using DFT methods for the compounds Si_5H_4, $Si_5(SiH_3)_4$ and $Si_5(SiMe_3)_4$.[28]

The C_2-symmetric **2** was investigated by multinuclear NMR spectroscopy in PhMe-d_8 and THF-d_8. The absence of hydride substituents at Si2, Si4 was evidenced by a 2D correlated ^{29}Si/^{1}H experiment (Fig. S26†) and by a quantitative ^{1}H NMR spectrum that revealed no hydride signal between 4 and 6 ppm. In the ^{1}H NMR spectrum at 300 K signal broadening is observed indicating dynamic behavior of **2** in solution. In the ^{29}Si NMR spectrum at 300 K signals at 94.2 ppm for Si1 and Si3, at 7.7 ppm for Si5 and Si6 and at −309.4 ppm for Si2 and Si4 appear in THF-d_8 besides signals at 7.0 and 7.4 ppm for the two chemically and magnetically different SiMe$_3$ groups. These measured signals are in good accordance with DFT calculated values (see Table S4†). The signal at very high field for the unsubstituted Si atoms at −309.4 ppm is in line with that observed for this type of atoms in **F** and **D** (−273.2 and −274.2 ppm, respectively). The dynamic behavior of **2** was analyzed by variable temperature (VT) ^{1}H NMR spectroscopy, 2D
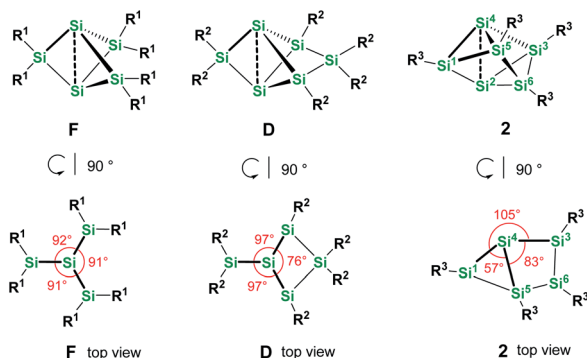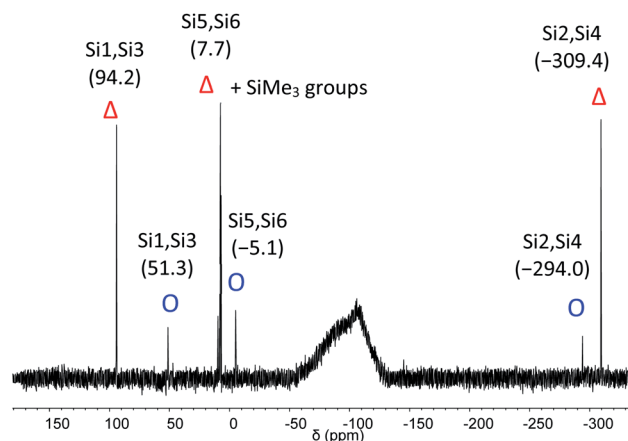

Fig. 3 ^{29}Si NMR spectrum of **2** in THF-d_8 at 210 K. Δ represents the major component and O the minor component.

NMR experiments and lineshape analysis. This analysis revealed that two species in a 2 : 1 ratio are in equilibrium with each other (see Fig. 3, S19 and page S42†). The minor component has three signals in the ^{29}Si NMR spectrum at 51.3, −5.1 and −294.0 ppm.

Examination of **2** *via* solid state ^{29}Si{^{1}H} CP/MAS NMR spectroscopy was performed, confirming that only the major component is present in the solid state signals at $\delta = 98.7$, 8.9 and −301.2 ppm, besides two ^{29}Si signals at $\delta = 7.4$ and 6.6 ppm for the SiMe$_3$ groups (see Fig. 4). The solid-state ^{29}Si chemical shifts differ slightly from the solution state shifts, most likely due to ring current effects of the aromatic ligands in the solid, which are averaged out by motion in solution. In the solid-state, the ^{29}Si chemical shift anisotropy (CSA)[29] supported by DFT calculations can be used for signal assignment. The ^{29}Si CSAs were determined from analysis of the spinning sidebands at low spinning speed (4.0 kHz MAS, see Fig. 4b). The ^{29}Si signals of the SiMe$_3$ groups at $\delta = 6.6$ and 7.4 ppm show the smallest CSA ($\delta_{aniso} = 20 \pm 10$ ppm) as expected and in good agreement with DFT calculations (see Table S9†). The two unsubstituted silicon atoms (Si2/4) correspond to the ^{29}Si resonance at $\delta = -301$ ppm. The low ^{29}Si CSA of $\delta_{aniso} = 95 \pm 10$ ppm with $\eta_\sigma = 0.25$ for these

Fig. 2 Comparison of the configuration of the ligand-free silicon atoms in **F**, **D** and **2**.
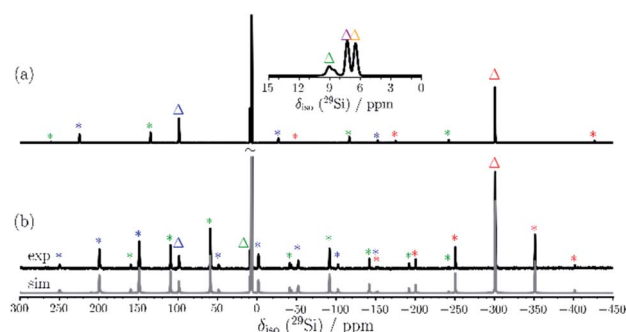

Fig. 4 ^{29}Si{^{1}H} CP/MAS NMR spectra of **2** recorded at 9.4 T employing (a) 10.0 kHz and (b) 4.0 kHz MAS. The inset in (a) enlarges the chemical shift region of the SiMe$_3$ groups. The corresponding fit is shown in grey in (b). The isotropic ^{29}Si resonances are marked by triangles and spinning sidebands are marked with an asterisk.

two atoms suggests only a weak coordination between these silicon atoms, since the distance (2.636(6) Å) is significantly longer than a Si–Si single bond (2.34 Å). The ^{29}Si signals of Si1/3 at $\delta = 99$ ppm and Si5/6 at $\delta = 9$ ppm show similar ^{29}Si CSA values ($\delta_{aniso} = -230 \pm 20$ ppm and -226 ± 20 ppm, respectively) in accordance with DFT calculations ($\delta_{aniso} = -284$ ppm and -297 ppm). Here, Si1/3 have $\eta_\sigma = 0.1$ whereas Si5/Si6 show an axial symmetric tensor with $\eta_\sigma = 0$. These differences in ^{29}Si CSA parameters can be understood by comparing the different bonding situations at Si5/6 in contrast to Si1/Si3.

The bond lengths involving Si5/Si6 are all very similar whereas those of Si1/Si3 include the two short bonds (2.292(6) and 2.281(5) Å) to the adjacent Si2/Si4 atoms and the longer bonds to Si4/Si2 (2.532(6) and 2.502(6) Å), respectively. This results in a non-axial ^{29}Si CSA tensor for Si1/Si3. The slight discrepancy between experiment and calculations of ^{29}Si δ_{aniso} values for Si1–Si6 may indicate that some residual local mobility is present even in the solid state.

The experimental UV Vis spectrum of **2** at room temperature shows a shoulder at 361 nm and at 314 nm. These absorptions can be assigned to a HOMO−1 → LUMO transition and a HOMO → LUMO+1 transition, respectively, according to TDDFT calculation with ORCA on the optimized structure (**2-A**) of Si$_6${N(SiMe$_3$)Dipp}$_4$, using the CAM-B3LYP functional, a double zeta basis set (def2-SVP) and the CPCM implicit solvent model for toluene (page S28).† The HOMO–LUMO transition at 392 nm is very weak and cannot be identified in the experimental spectrum.

Quantum theory of atoms in molecules (QTAIM)[30] analysis was performed to elucidate more precisely the bonding situation of **2**. According to this analysis bond critical points, represented as green circles in Fig. 5 (and Fig. S3†), exist between all bonds except for that connecting the two ligand-free silicon atoms (Si2 and Si4). This was also observed for the

benzpolarene-type cluster **D** and the tricyclic hexasilabenzene isomer **C**.[31]

Additionally, Mayer bond orders[32] (Table S3†) were determined that indicate highest bond orders for the Si1–Si5, Si3–Si6 bonds (0.90) from the butterfly-shaped ring to the Si5–Si6-dumbbell and for the two short bonds Si1–Si2 and Si3–Si4 in the upper butterfly-shaped ring (0.86). The bond order of the transannular distance Si2···Si4 (0.46) is only half as much and does not differ greatly from that of the long bonds Si2–Si3 and Si1–Si4 (0.52) in the four-membered butterfly ring composed of Si1–Si2–Si3–Si4.

The Si–N bonds have bond orders of (1.11 and 1.02). This demonstrates that the amine substituents are very weak π-donors and strong σ-acceptors. Additionally, the molecular orbitals do not include Si=N π-bonds (see Fig. S4†). Together with the trigonal planar configuration at the N atoms, stabilized by the large substituents, this suggests, that to some degree negative hyperconjugation between the p-type lone pair at each N atom and the antibonding σ*-orbitals of the Si–Si bonds occurs.

An intrinsic bond orbital (IBO)[33] analysis of **2** was conducted with a double zeta basis set (def2-SVP) and gave IBOs in the Si$_6$ core as shown in Fig. 5 and S5.† This analysis reveals 10 IBOs relevant for the Si$_6$ cluster core. This corresponds to 20 cluster electrons, which is in line with the four amido-substituted silicon atoms contributing each three electrons to the cluster, and the two ligand-free silicon atoms that each provide four electrons. In particular, we note seven single σ-bonds (IBO 291–297), that include all Si–Si bonds except the Si1–Si4 and Si2–Si3 bonds and the transannular distance between Si2 and Si4. Furthermore, lone pairs on Si2 and Si4 (IBO 299 and 300) and a multi-center bond at the butterfly-shaped ring (IBO 298) turned out from this analysis. The multi-center bond explains the observed partial double bond character of the Si1–Si2/Si3–Si4 bonds and the partial σ-bonds between Si1–Si4, Si2–Si3 and Si2···Si4 (dashed lines in Fig. 1). According to these findings, the molecular structure **2** carries a certain contribution of the resonance structures represented in Fig. 6. These resonance structures indicate somewhat the analogy of **2** to the butalene-type isomer C$_6$H$_4$ which was recently reinvestigated.[34]

The three signals in the ^{29}Si NMR spectrum in THF-d_8 of the minor component **2-C** at 51.3, −5.1 and −294.0 ppm indicate that this component is also C_2 symmetric. Two of the signals (at −5.1 and at −294.0 ppm) are very close to the major component. This provides strong evidence, that the minor component is very similar to the major component. The occurrence of a major and a minor isomer with different chemical shifts in solution was recently also observed for anionic mixed silicon germanium
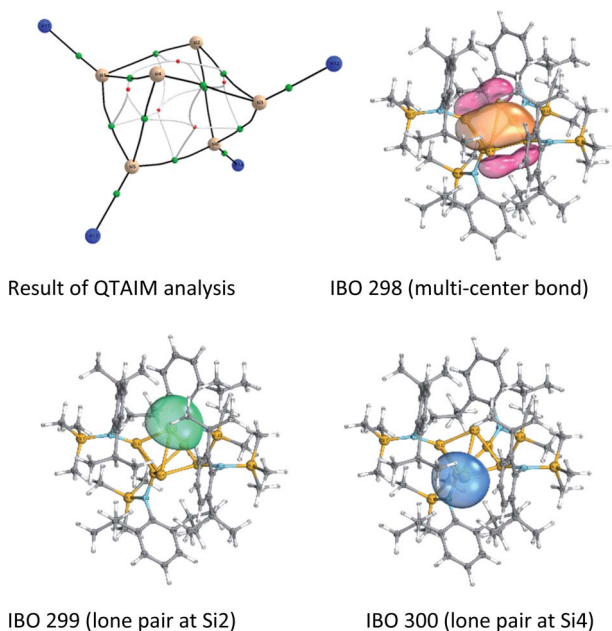

Result of QTAIM analysis

IBO 298 (multi-center bond)

IBO 299 (lone pair at Si2)

IBO 300 (lone pair at Si4)

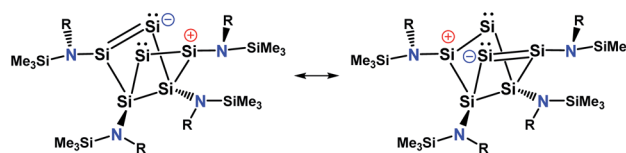**Fig. 5** Result of the QTAIM analysis and IBOs 298, 299 and 300.

**Fig. 6** Possible resonance structure of **2**.

benzpolarene-type clusters.[35] Lineshape analysis revealed a non-mutual exchange between the two components and a Gibbs free energy of activation of 57.2 kJ mol^{-1} (13.7 kcal mol^{-1}) at 300 K for the equilibrium between the major and the minor isomer (see page S42 and S43†).

With this information we generated conformational isomers of **2** by rotating the ligands successively around the Si$_{Cluster}$–N single bonds in steps of 60° and optimizing the structures with DFT calculations. From the generated set of conformers, only the four most stable are reported here (Scheme 5).

Conformer **2-B** results from counterclockwise rotation around the Si5–N bond. Conformer **2-C** is obtained when the Si6–N bond from **2-B** is rotated clockwise. The enantiomer of **2-A**, which is conformer **2-D**, can be generated by a twist within the four-membered ring Si2–Si4–Si5–Si6 of the Si$_6$ scaffold in conformer **2-C** (Scheme S1†). This is accompanied by a slight movement of the amine substituents attached to the butterfly-shaped ring. We note that both enantiomers **2-A** and **2-D** are present in the crystal structure obtained from single crystals grown from hexane. Conformers in which the substituents of Si1 and Si3 were rotated around the Si$_{cluster}$–N bond were found to have significantly higher (>7 kcal mol^{-1}) relative free energies and are not discussed. The relative free energies, obtained with PW6B95-D3 and DLPNO-CCSD(T) are given in Table S1.† Calculations of chemical shifts for these isomers revealed that those of the C_2-symmetric isomer **2-C** (57.5, −15.9, −273.4 ppm, Table S4†) display very good agreement with those measured for the minor component in THF-d_8 at 210 K (51.3, −5.1 and −294.0 ppm).

In order to get an estimate for the (electronic) potential barriers of each step and to find out whether these transformations proceed stepwise or concertedly, three optimizations of the minimum energy path between conformers **2-A**, **2-B**, **2-C** and **2-D** (=ent-**2-A**) were conducted. The growing string method (GSM)[36] was applied to construct these paths from **2-A** to **2-D**. The three minimum energy paths were connected to a complete path as shown in Fig. 7.

We found, that the barriers for ligand rotation both lie well below 20 kcal mol^{-1}, which is in accord with the result obtained
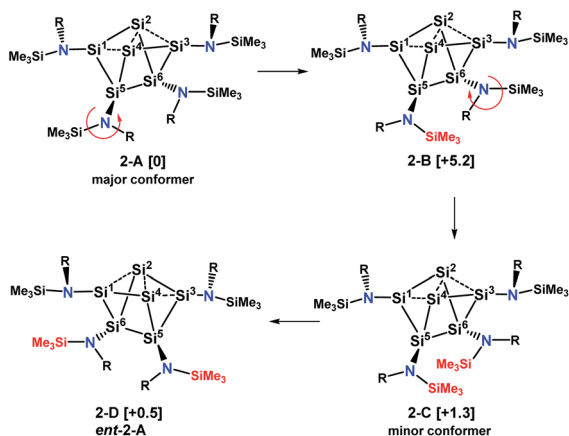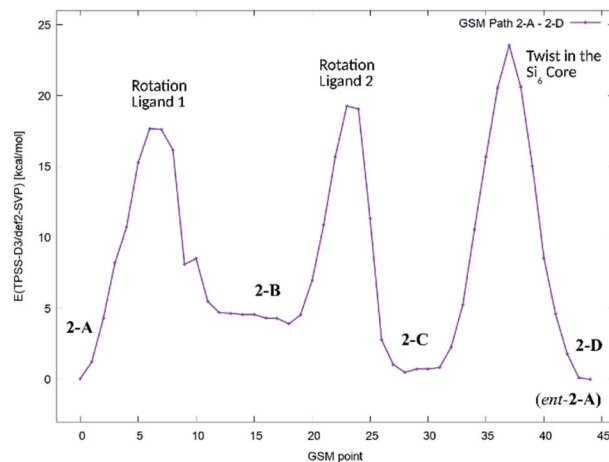

Fig. 7 Potential energy diagram (TPSS-D3/def2-SVP) of the minimum energy path for the stepwise transformation of **2-A** to the minority conformer **2-C** and the formation of the enantiomer of **2-A** (**2-D**).

from lineshape analysis. The subsequent twist in the Si2–Si4–Si5–Si6 ring has to overcome an (electronic) energy barrier of approximately 24 kcal mol^{-1}. Attempts to optimize reaction paths of the synchronous (symmetric) rotation of two ligands (**2-A → 2-C**) and eventually including the twist in the Si2–Si4–Si5–Si6 ring (**2-A → 2-D**) results in paths with significantly higher potential energy barriers.

Additionally, molecular dynamics (MD) simulations with the ReaxFF force field[37] were performed for the four DFT-optimized structures **2-A**, **2-B**, **2-C** and **2-D**. In order to qualitatively assess the formation mechanism of the enantiomer **2-D** starting from structure **2-A**, a targeted MD simulation[38] was performed slowly pulling the system from **2-A** to **2-D** over a duration of 2 ns. A video visualizing this process is available via the ESI link.†

In this simulation, the necessary structural changes, i.e. rotation of a first ligand, rotation of a second ligand, and distortion within the Si$_6$ cluster core, occur sequentially one after another. This suggests that the transformation **2-A → 2-D** takes place by a stepwise process via structures **2-B** and **2-C**, supported by the clearly visible minima in the free energy profile (Fig. S7†). The barrier heights for the individual processes (Table S5 and Fig. S8†) are well below $\Delta F^{\ddagger} = 12$ kcal mol^{-1}. They are thus easily accessible at $T = 300$ K. In particular, if both enantiomers, **2-A** and **2-D**, are present, two competing pathways, **2-A → 2-C** and **2-D → 2-C**, are possible.

The reactivity of **2** with ethylene, CO_2, CCl_4, H_2O, MeOH, I_2 and NHC^{Me_4} (2,3,4,5-tetramethyl-imidazolium-2-ylidene) was investigated in NMR scale reactions. But, these reagents either show no reactivity with **2** (ethylene, CO_2, MeOH) or react very unselectively (CCl_4, H_2O, I_2, NHC^{Me_4}) which hinders characterization of the products based only on NMR spectroscopy and the growths of single crystals in solution.

Scheme 5 Major and minor conformer and enantiomer of **2** in solution. Values in brackets are solvent corrected relative free energies $\Delta G(298)_{solv}$.

Conclusions

In summary, we synthesized a highly unsaturated Si$_6$ cluster with only four amine substituents and two ligand-free silicon

atoms that exhibits an unusual equilibrium in solution between a major and a minor conformer. Variable temperature and 2D-correlated NMR experiments, DFT calculations and molecular dynamics simulations were performed to collect information on this process. These calculations suggest, that the equilibration of the two conformers detected in solution by NMR spectroscopy of **2** (**2-A** and **2-C**) may occur at room temperature by two subsequent ligand rotations or by a twist in the Si_6 core. Analysis of the bonding situation in the Si_6 cluster using the QTAIM method revealed no bond critical point between the ligand-free silicon atoms. Generating intrinsic bond orbitals (IBOs) for the Si_6 cluster core demonstrates lone pair type character at the ligand free silicon atoms and a multi-center bond involving all silicon atoms in the butterfly-shaped ring. In future experiments, the potential of amine substituents for the stabilization of other highly unsaturated silicon clusters will be investigated.

Conflicts of interest

There are no conflicts to declare.

Acknowledgements

Notes and references

1 (a) A. Sekiguchi, T. Yatabe, C. Kabuto and H. Sakurai, *J. Am. Chem. Soc.*, 1993, **115**, 5853; (b) K. Abersfelder, A. Russell, H. S. Rzepa, A. J. P. White, P. R. Haycock and D. Scheschkewitz, *J. Am. Chem. Soc.*, 2012, **134**, 16008.

2 (a) A. Tsurusaki, C. Iizuka, K. Otsuka and S. Kyushin, *J. Am. Chem. Soc.*, 2013, **135**, 16340; (b) S. Ishida, K. Otsuka, Y. Toma and S. Kyushin, *Angew. Chem., Int. Ed.*, 2013, **52**, 2507.

3 K. Abersfelder, A. J. P. White, H. S. Rzepa and D. Scheschkewitz, *Science*, 2011, **327**, 564.

4 K. Abersfelder, A. J. P. White, R. J. F. Berger, H. S. Rzepa and D. Scheschkewitz, *Angew. Chem., Int. Ed.*, 2011, **50**, 7936.

5 M. Moteki, S. Maeda and K. Ohno, *Organometallics*, 2009, **28**, 2218.

6 Y. Heider, N. E. Poitiers, P. Willmes, K. I. Leszczyńska, V. Huch and D. Scheschkewitz, *Chem. Sci.*, 2019, **10**, 4523.

7 T. Iwamoto and S. Ishida, *Chem. Lett.*, 2014, **43**, 164.

8 Y. Heider and D. Scheschkewitz, *Dalton Trans.*, 2018, **47**, 7104.

9 (a) J. M. Buriak, *Chem. Rev.*, 2002, **102**, 1271; (b) N. T. K. Thanh, N. Maclean and S. Mahiddine, *Chem. Rev.*, 2014, **114**, 7610; (c) P. Munnik, P. E de Jongh and K. P. de Jong, *Chem. Rev.*, 2015, **115**, 6687.

10 (a) A. Schnepf, *Chem. Soc. Rev.*, 2007, **36**, 745; (b) A. Schnepf, *Angew. Chem., Int. Ed.*, 2004, **43**, 664; (c) A. Schnepf, *New J. Chem.*, 2010, **34**, 2079.

11 (a) C. Hollenstein, *Plasma Phys. Contr. Fusion*, 2000, **42**, R93–R104; (b) F. Zhang, K. Sautter, A. M. Larsen, D. A. Findley,

R. C. Davis, H. Samha and M. R. Linford, *Langmuir*, 2010, **26**, 14648.

12 D. Scheschkewitz, *Angew. Chem., Int. Ed.*, 2005, **44**, 2954.

13 D. Nied, R. Köppe, W. Klopper, H. Schnöckel and F. Breher, *J. Am. Chem. Soc.*, 2010, **132**, 10264.

14 K. Leszczyńska, V. Huch, C. Präsang, J. Schwabedissen, R. J. F. Berger and D. Scheschkewitz, *Angew. Chem., Int. Ed.*, 2019, **58**, 5124.

15 N. Akasaka, S. Ishida and T. Iwamoto, *Inorganics*, 2018, **6**, 107.

16 (a) N. Wiberg, C. M. M. Finger and K. Polborn, *Angew. Chem., Int. Ed.*, 1993, **32**, 1054; (b) N. Wiberg, C. M. M. Finger, H. Auer and K. Polborn, *J. Organomet. Chem.*, 1996, **521**, 377.

17 T. Iwamoto, N. Akasaka and S. Ishida, *Nat. Commun.*, 2014, **5**, 5353.

18 P. Willmes, K. Leszczyńska, Y. Heider, K. Abersfelder, M. Zimmer, V. Huch and D. Scheschkewitz, *Angew. Chem., Int. Ed.*, 2016, **55**, 2907.

19 Y. Heider, P. Willmes, V. Huch, M. Zimmer and D. Scheschkewitz, *J. Am. Chem. Soc.*, 2019, **141**, 19498.

20 P. M. Warner and G. B. Jones, *J. Am. Chem. Soc.*, 2001, **123**, 10322.

21 M. Iannuzzi, A. Laio and M. Parrinello, *Phys. Rev. Lett.*, 2003, **90**, 238302.

22 (a) A. J. Adamczyk and L. J. Broadbelt, *J. Phys. Chem. A*, 2011, **115**, 8969; (b) T. Miyazaki, T. Uda, I. Stich and K. Terakura, *Chem. Phys. Lett.*, 1996, **261**, 346.

23 M. Lappert, A. Protchenko, P. Power, and A. Seeber, *Metal Amide Chemistry*, Wiley-VCH, 2008.

24 M. Brynda, R. Herber, P. B. Hitchcock, M. F. Lappert, I. Nowik, P. P. Power, A. V. Protchenko, A. Růžička and J. Steiner, *Angew. Chem., Int. Ed.*, 2006, **45**, 4333.

25 J. Keuter, K. Schwedtmann, A. Hepp, K. Bergander, O. Janka, C. Doerenkamp, H. Eckert, C. Mück-Lichtenfeld and F. Lips, *Angew. Chem., Int. Ed.*, 2017, **56**, 13866.

26 (a) P. P. Power, *Chem. Rev.*, 1999, **99**, 3463; (b) A. Sekiguchi and V. Y. Lee, *Chem. Rev.*, 2003, **103**, 1429.

27 M. Kaftory, M. Kapon, and M. Botoshansky, *The Chemistry of Organic Silicon Compounds*, ed. Z. Rappoport and Y. Apeloig, Wiley, Chichester, 1998, vol. 2.

28 V. Y. Lee, Y. Ito, O. A. Gapurenko, A. Sekiguchi, V. I. Minkin, R. M. Minyaev and H. Gornitzka, *Angew. Chem., Int. Ed.*, 2015, **54**, 5654.

29 The CSA parameters are defined as $\delta_{iso} = \frac{1}{3}(\delta_{xx} + \delta_{yy} + \delta_{zz})$, $\delta_\sigma = \delta_{iso} - \delta_{zz}$, $\eta_\sigma = (\delta_{xx} + \delta_{yy})/\delta_\sigma$, with $|\delta_{zz} - \delta_{iso}| \geq |\delta_{xx} - \delta_{iso}| \geq |\delta_{yy} - \delta_{iso}|$. The asymmetry parameter η_σ describes the symmetry of the CSA tensor. The CSA tensor is axial symmetric if $\eta_\sigma = 0$ and deviates from axial symmetry for $0 < \eta < 1$.

30 R. F. W. Bader, *Atoms in Molecules – A Quantum Theory*, Oxford University Press, Oxford, 1990.

31 D. Kratzert, D. Leusser, J. J. Holstein, B. Dittrich, K. Abersfelder, D. Scheschkewitz and D. Stalke, *Angew. Chem., Int. Ed.*, 2013, **52**, 4478.

32 I. Mayer, *Chem. Phys. Lett.*, 1983, **97**, 270.

33 (a) G. Knizia, *J. Chem. Theory Comput.*, 2013, **9**, 4834; (b) G. Knizia and J. E. M. N. Klein, *Angew. Chem., Int. Ed.*, 2015, **54**, 5518.

34 D. L. Cooper, P. B. Karadakov and B. J. Duke, *J. Phys. Chem. A*, 2015, **119**, 2169.

35 L. Klemmer, V. Huch, A. Jana and D. Scheschkewitz, *Chem. Commun.*, 2019, **55**, 10100.

36 P. M. Zimmerman, *J. Chem. Phys.*, 2013, **138**, 184102.

37 (*a*) K. Chenoweth, A. C. T. van Duin and W. A. Goddard, *J. Phys. Chem. A*, 2008, **112**, 1040; (*b*) H. M. Aktulga, J. C. Fogarty, S. A. Pandit and A. Y. Grama, *Parallel Comput.*, 2012, **38**, 245; (*c*) A. D. Kulkarni, D. G. Truhlar, S. Goverapet Srinivasan, A. C. T. van Duin, P. Norman and T. E. Schwartzentruber, *J. Phys. Chem. C*, 2013, **117**, 258; (*d*) G. Barcaro, S. Monti, L. Sementa and V. Carravetta, *J. Chem. Theory Comput.*, 2017, **13**, 3854.

38 (*a*) J. Schlitter, W. Swegat and T. Mülders, *J. Mol. Model.*, 2001, **7**, 171; (*b*) J. Schlitter and M. Klähn, *Mol. Phys.*, 2003, **101**, 3439.